JOURNAL OF CATALYSIS 147, 465–475 (1994)

Changes in the Structure of TiO_2-Supported Molybdena Induced by Na-Doping

C. Martin, I. Martin, and V. Rives

Departamento de Química Inorgánica, Universidad de Salamanca, Facultad de Farmacia, 37007 Salamanca, Spain

and

P. Malet

Departamento de Química Inorgánica, Instituto de Ciencia de Materiales, Universidad de Sevilla, C.S.I.C., 41012 Sevilla, Spain

Received July 30, 1993; revised December 8, 1993

The structure of well-dispersed molybdena moieties on the surface of a MoO_3–TiO_2 sample has been determined by extended X-ray absorption fine structure (EXAFS) spectroscopy. Octahedral coordination of molybdenum atoms is favored over the TiO_2 support, and [MoO_6] units join edges to form molybdenum rows that are similar to those found along the *c*-axis direction in bulk MoO_3. The changes induced in this structure when the support is doped with different amounts (1, 3% w/w) of sodium have been studied by X-ray diffraction, temperature programmed reduction, and infrared and EXAFS spectroscopies. The addition of Na changes the coordination of Mo^{6+} ions from octahedral to tetrahedral, and simultaneously inhibits their reducibility. Mo–Mo bonds found in the Na-free sample are broken, and at low Na content isolated MoO_4^{2-} units and ill-crystallized $Mo_2O_7^{2-}$ chains are formed. Increasing the amount of the Na dopant increases the fraction of Mo atoms in tetrahedral coordination and crystalline $Na_2Mo_2O_7$ coexists with dispersed phases in the 3% Na w/w sample. Also, an increase in the calcination temperature of the samples leads to the formation of crystalline Na–Mo–O compounds over the TiO_2 surface.

INTRODUCTION

Molybdena–titania catalysts are excellent for the selective oxidation of hydrocarbons (1) and for the oxidative dehydrogenation of alcohols (2), as well as for the selective catalytic reduction of NO_x by ammonia (3). Moreover, they are also precursors of alkene metathesis catalysts (4) and of sulfided hydrodesulfurization catalysts (5). The activity and selectivity of molybdena supported systems is deeply modified by the structure and physicochemical properties of the dispersed moieties supported on the surface (6), which can be affected by parameters such as preparation conditions, nature of the support, active phase contents, and addition of dopants. Thus, molybdena spreads more readily on the TiO_2 surface than in Al_2O_3 or SiO_2 supports (7), and Eon *et al.* (8) have suggested that molybdena–titania interaction takes place through a perfect adjustment of (010) planes of MoO_3 with (001) planes of TiO_2, thus leading to an epitaxial growth in the (0*k*0) direction of MoO_3 crystals over the TiO_2. Also, the coordination symmetry around Mo atoms that form the active sites is influenced by the support, and a recent X-ray absorption fine structure (XAFS) study (9) concludes that while the predominant structure of molybdate on the Al_2O_3 support changes from tetrahedral to octahedral with increasing Mo loading, a MoO_3-like structure is formed on the SiO_2 support, and dispersed Mo atoms in octahedral coordination are favored over TiO_2. Results from this study are in agreement with previous data (10, 11) which indicate that isolated tetrahedra (MoO_4^{2-}) are formed only on the basic OH groups on the surface of alumina, and when the metal loading rises above a critical concentration an octahedral polymolybdate is formed (11–13). A high dispersion of octahedral polymolybdate over the titania surface was found by Ng and Gulari (14), who used laser raman and IR spectroscopies, and was also suggested by ESR and XPS results (15). However, although two-dimensional polymolybdate structures over the TiO_2 surface are suggested by these studies, no information has been reported about the degree and way of agglomeration of the basic octahedral units to form the structure of the dispersed moieties.

The employment of alkaline metals as promoters has been described when MoO_3 is supported on alumina (16, 17), and changes in the coordination of Mo^{6+} species from octahedral to tetrahedral induced by the presence of these dopants have been proposed. Thus, O'Young (16) suggests that suppression of the reducibility of Mo^{6+} species

0021-9517/94 $6.00

and of the NO uptake at high Alk/Mo atomic ratios (Alk = K, Cs; Alk/Mo > 2) could be due to the formation of K_2MoO_4 or Cs_2MoO_4 on the surface. However, no direct evidence of the formation of these compounds is found. At lower Alk/Mo atomic ratios the interaction between molybdenum and the promoter decreases, although both the reducibility and NO uptake still decrease significantly. Also, Kantschewa *et al.* (17) found a strong interaction of potassium with the support surface and the molybdate phase when comparing $NiMo/Al_2O_3$ and $KNiMo/Al_2O_3$ catalysts. These authors report that the original octahedral coodination of Mo^{6+} in the $NiMo/Al_2O_3$ catalysts is transformed into a tetrahedral coordination and the reducibility of Mo^{6+} is strongly decreased in the presence of K^+ ions. A significant reduction in activity was observed for hydrodesulfurization in the presence of K^+ ions, while the activity in the water gas shift reaction was simultaneously enhanced.

In the present paper a set of monolayer MoO_3 catalysts supported over TiO_2 and doped with different amounts (1, 3% w/w) of sodium have been characterized by means of X-ray diffraction (XRD), temperature programmed reduction (TPR), and Fourier transform infrared (FTIR) and EXAFS spectroscopies, allowing us to obtain information about the structure of dispersed molybdena moieties over the TiO_2 surface, and the changes induced in this structure upon Na-doping.

EXPERIMENTAL

Sample Preparation

Titania support was P-25 from Degussa (Germany). After calcination overnight at 773 K to withdraw adsorbed organic impurities, different amounts of sodium (0, 1, or 3% w/w) were incorporated into titania by impregnation with aqueous solutions of NaOH (from Panreac, p.a.) in a rotavapor in order to avoid formation of carbonates. After drying and calcination in air at 773 K for 3 h, the doped support was impregnated with an aqueous solution of ammonium heptamolybdate (AHM) from Fluka; the amounts of solid and solution were chosen in order to incorporate the amount of molybdenum equivalent to the formation of one "geometrical" monolayer of molybdena on the titania support after calcination. This value was calculated from the specific surface area of the support (53 ± 2 m^2 g^{-1}) and the area covered by a "molecule" of MoO_3, 15×10^4 pm^2 (18). The impregnated solids were dried at 383 K for 24 h and calcined in air at 773 or 1100 K for 3 h. The first temperature is high enough to decompose AHM to molybdena, and the last one permits melting of molybdena and, we expect, its dispersion on the support surface. For comparison purposes, portions of the unloaded supports were also submitted to treatment under similar conditions. Supports are named Ti/%Na (w/w)/calcination temperature (K), while molybdena loaded samples are named Mo/Ti/%Na(w/w)/calcination temperature (K).

Bulk MoO_3, $Na_2MoO_4 \cdot 2H_2O$, and $Na_2Mo_2O_7$ were used as reference compounds. MoO_3 was obtained by calcining AHM at 773 K. $Na_2MoO_4 \cdot 2H_2O$ was commercial (Fluka p.a.). $Na_2Mo_2O_7$ was made (19) by intimately mixing in a porcelain crucible equimolar amounts of molybdenum (VI) oxide and sodium ortomolybdate, which were then fused at 800°C for 12 h. The melt was then quenched by pouring onto cold porcelain and, after grinding, was stored in a desiccator. IR spectra and XRD data for the product agreed with those previously reported (20, 21).

Experimental Procedures

Chemical analysis for molybdenum was performed by atomic absorption (AA) in an ELL-240 Mark-2 instrument. XRD profiles were recorded in a Phillips PW 1070 instrument, using Ni-filtered Cu$K\alpha$1 radiation (λ = 154.05 pm). Nitrogen adsorption measurements at 77 K for surface area and porosity assessment were carried out in a conventional high vacuum pyrex system (residual pressure 10^{-4} N m^{-2}), pressure changes being monitored with a MKS pressure transducer. FTIR spectra were recorded in a Perkin–Elmer FTIR 1730 spectrometer, using KBr disks, with a nominal resolution of 4 cm^{-1} and averaging 100 spectra. A KBr disk with the same weight of unloaded support was used to record the background spectrum, in order to cancel all absorption bands originated by the support. TPR profiles were recorded in a conventional, homemade apparatus with a catharometric detector using a 5% H_2/Ar mixture (from Sociedad Española del Oxigeno, S.A., Spain) as the carrier gas, with a flow of 50 ml/min and a heating rate of 10 K/min. The amount of sample reduced (ca. 160 mg) corresponds to 100 μmol Mo, thus ensuring good resolution under the experimental conditions employed (22). Calibration with CuO and other details of the procedure have been reported elsewhere (22). X-ray absorption (XAS) data were collected on wiggler station 9.2 at the Synchrotron Radiation Source in Daresbury (United Kingdom) with a beam of 2 GeV and 210–230 mA. Monochromatization was obtained with a double silicon crystal working at the (200) reflection detuned 50% to minimize higher harmonics. The measurements were carried out in transmission mode using optimized ion chambers as detectors. Supported samples were ground and homogenized, and precalculated amounts were pressed into self-supporting wafers with a mass absorption coefficient μ_x 2.5 cm^{-1} ($\Delta\mu_x < 1$ just above the Mo*K* edge, 20,005 eV). Crystalline compounds were diluted with boron nitride (Merck) and prepared in the same way. Samples were placed in an *in situ* cell and Mo*K* spectra were measured under helium atmosphere

at high liquid nitrogen temperature after purging with helium at room temperature for 1 h. At least three scans were recorded and averaged in order to obtain the experimental spectra. The EXAFS function was obtained from the experimental X-ray absorption spectrum by conventional procedures (23). EXAFS data handling and analysis was performed by using the program package NEWEXAFS from the Eindhoven University of Technology.

RESULTS

Chemical Analysis, X-Ray Diffraction, and Nitrogen Adsorption

Chemical analysis results for molybdenum are included in Table 1, together with the specific surface area values (S_{BET}) and the anatase contents in the samples, as determined from the relative intensities of the most intense X-ray diffraction peaks due to anatase and rutile following the equation given by Criado and Real (24).

Chemical analysis data indicate that calcination at 773 K has no significant effect on the molybdenum content, while calcination at 1100 K leads to a partial removal of molybdenum, probably by sublimation as MoO_3, this removal being higher in the absence of sodium; so, only 20% of the initial amount of Mo remains in sample Mo/Ti/0/1100, while 75% is still present in sample Mo/Ti/3/1100. Therefore, molybdenum is stabilized over the Na-doped TiO_2 support.

With regard to the anatase/rutile phase change, the anatase content in the parent support is ca. 50%. Calcination at 773 K has only minor effects, the anatase content slightly decreasing upon incorporation of Mo and/or Na. A parallel decrease in the specific surface areas of the samples is observed (Table 1). Therefore, both effects (rutilization and sintering) seem to have the same origin. Changes are more evident in the samples calcined at 1100 K. So, all titania exists in the rutile phase, the diffraction peaks originated by anatase being vanished in all the samples under study. Specific surface areas are also very much lower than for similar samples calcined at 773 K. Thus, for Na-free samples the value obtained was 9.4 m^2/g, ca. 18% of the original S_{BET} value, while for samples containing sodium the specific surface area was almost below the instrumental measuring limit.

TABLE 1

Summary of Characterization Results for the Samples Studied

Sample	% Na	% Mo	S_{BET} (m^2/g)	% Anatase
Ti/0/773	0	0	52.5	55
Ti/1/773	1	0	47.1	55
Ti/3/773	3	0	44.8	51
Mo/Ti/0/773	0	5.8	41.5	52
Mo/Ti/1/773	1	5.8	39.2	50
Mo/Ti/3/773	3	5.8	38.2	51
Ti/0/1100	0	0	9.4	0
Ti/1/1100	1	0	<1	0
Ti/3/1100	3	0	<1	0
Mo/Ti/0/ 1100	0	1.2	9.4	0
Mo/Ti/1/ 1100	1	n.m.	<1	0
Mo/Ti/3/ 1100	3	4.5	<1	0

Note. n.m., not measured.

In addition to diffraction peaks of anatase and rutile, some other diffraction maxima, although very weak, are recorded in the profiles of the samples. For the Mo-free supports weak peaks due to Na_4TiO_4 are detected only in the diffraction profiles of sample with 3% w/w Na calcined at 1100 K; all other Mo-free samples show only diffraction peaks due to anatase and/or rutile. For the sample Mo/Ti/0/773 a weak peak due to MoO_3 (110) planes is recorded at 381 pm, the other main peaks of this compound being overlapped by those due to titania. The low intensity of this peak, when compared with that obtained for an uncalcined, 5.8% w/w Mo physical mixture MoO_3 + TiO_2, indicates a high dispersion degree of the molybdena over the support surface in the impregnated sample after calcination at 773 K. This MoO_3 peak is no longer recorded (Fig. 1) in the profiles of Na-doped sam-

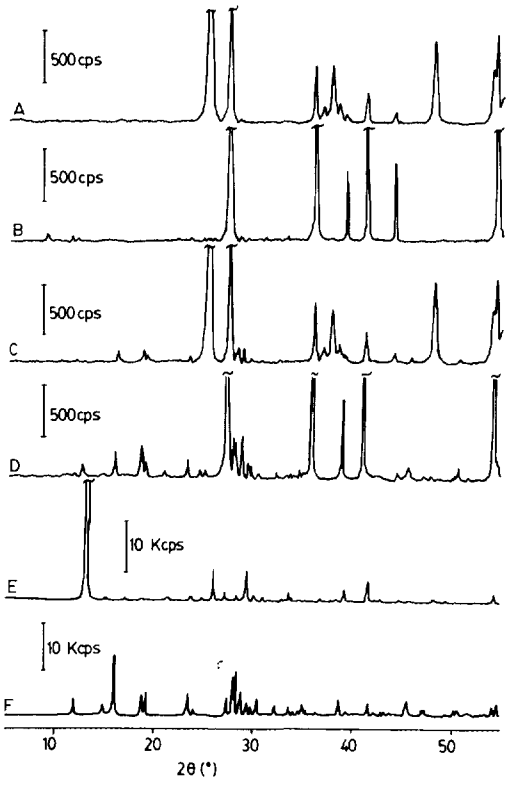

FIG. 1. X-ray diffraction patterns of Na-doped MoO_3/TiO_2 supported samples (A) Mo/Ti/1/773, (B) Mo/Ti/1/1100, (C) Mo/Ti/3/773, and (D) Mo/Ti/3/1100. XRD patterns of crystalline (E) $Na_2MoO_4 \cdot 2H_2O$ and (F) $Na_2Mo_2O_7$ have been included for comparison.

TABLE 2

X-Ray Diffraction Data of Surface Compounds and Selected References[a]

Sample	d (pm)											
Mo/Ti/1/773					[b]	[c]	312					
Mo/Ti/3/773	549	471		378	[b]	[c]	313	307		198	179	
Mo/Ti/1/1100						[c]	312					
Mo/Ti/3/1100	551	472	463	379	361	[c]	315	307	301	198	180	167
$Na_2MoO_4 \cdot 2H_2O$					361	331	317	306	298			
$Na_2Mo_2O_7$	549	471	461	378		322	314	306	300	197		167

[a] XRD data for reference compounds from JCPDS-ICDD files, card numbers 34/76 ($Na_2MoO_4 \cdot 2H_2O$), and 22/906 ($Na_2Mo_2O_7$).
[b] Support peak at 351 pm: (101) planes of anatase.
[c] Support peak at 325 pm: (110) planes of rutile.

ples and calcined at 773 or 1100 K, where weak peaks that can be ascribed to Na–Mo–O compounds appear in addition to those of anatase and rutile. As shown in Table 2, due to the weakness of these peaks and to their overlapping, in some cases, with the intense peaks due to the support, ascription to a defined single phase is difficult. Thus, for samples doped with 1% Na w/w only a weak diffraction peak at 312 pm can be recorded, thus suggesting that most of the molybdenum present at the surface is well dispersed. This peak could be ascribed to the formation of small crystals of either $Na_2MoO_4 \cdot 2H_2O$ or $Na_2Mo_2O_7$, since both compounds have diffraction maxima near this value. As shown in Fig. 1, more complex and intense diffraction profiles are obtained for the samples doped with 3% Na w/w, thus indicating a poorer dispersion of the molybdenum compounds over the TiO_2 surface at this higher sodium content. From the position of these lines (Table 2) the formation of $Na_2Mo_2O_7$ is now evident, although the additional presence of $Na_2MoO_4 \cdot 2H_2O$ on the TiO_2 surface cannot be discarded.

FTIR Spectroscopy

FTIR spectra of the supported samples have been recorded. Since XRD suggests in some samples the formation of small amounts of crystalline MoO_3, $Na_2MoO_4 \cdot 2H_2O$, and $Na_2Mo_2O_7$, the spectra of these bulk compounds have been also recorded. Table 3 includes positions of the IR bands for the TiO_2 supported samples, as well as for the crystalline compounds. Distorted $[MoO_6]$ octahedra built layers in the MoO_3 structure, isolated $[MoO_4]$ tetrahedra are found in crystalline $Na_2MoO_4 \cdot 2H_2O$, and an equal number of $[MoO_4]$ and $[MoO_6]$ units form the chain structure of $Na_2Mo_2O_7$ (25a), thus giving rise to different Mo–O IR bands, as shown in Table 3.

For the Na-free samples loaded with a monolayer of MoO_3 only a broad absorption band at 990 cm^{-1} is detected, pointing to the presence of octahedral $[MoO_6]$ units similar to those found in MoO_3 on the surface of this sample. By doping the support with sodium this band disappears and a complex spectrum with several absorption bands in the 850–960 cm^{-1} range develops, indicating the formation of new molybdenum species on the support surface. In the samples doped with 3% Na w/w these bands are clearly resolved; they are almost independent of the calcination temperature and can be ascribed to the formation of $Na_2Mo_2O_7$ over the surface, in agreement with XRD results. In the samples doped with 1% Na w/w broad and ill-defined IR bands appear at similar positions, thus suggesting the incipient formation of the $Na_2Mo_2O_7$ complex chains, although they should be poorly crystallized since the XRD diffraction pattern of this compound was not clearly found in this sample, as reported above. Besides this, a band at ca. 900 cm^{-1}, characteristic of isolated $[MoO_4]$ units similar to those found in $Na_2MoO_4 \cdot 2H_2O$ is now evident in the IR spectra of 1% Na w/w samples.

Temperature Programmed Reduction (TPR)

TPR profiles for the two sets of samples here studied, as well as those of the crystalline compounds MoO_3, Na_2

TABLE 3

IR Bands in MoO_3/TiO_2–Na Samples and Reference Compounds

Compound	Bands (cm^{-1})						
MoO_3	989					879	
$Na_2MoO_4 \cdot 2H_2O$					900		858
$Na_2Mo_2O_7$		943	923	905		881	864
Mo/Ti/0/773	990						
Mo/Ti/1/773		938	923	910	897		
Mo/Ti/3/773		943	923	912		882	868
Mo/Ti/1/1100		956		911	893		870
Mo/Ti/3/1100		944	925	913		882	865

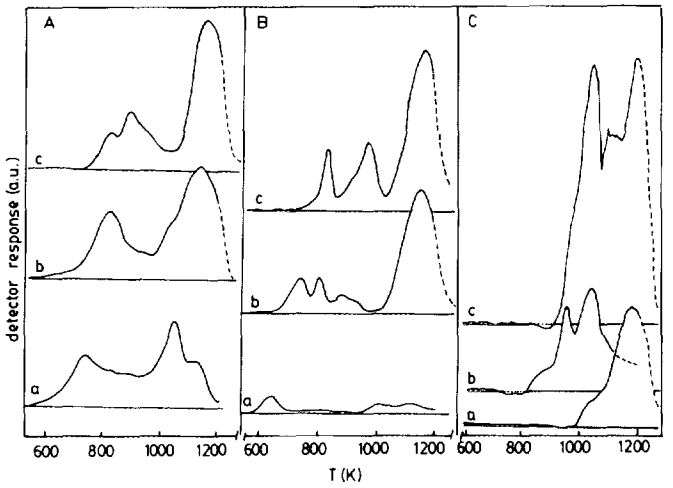

FIG. 2. Temperature programmed reduction profiles of MoO_3/TiO_2 supported samples calcined at 773 K (A) and 1100 K (B): (a) Na-free samples, (b) samples doped with 1% Na w/w, (c) samples doped with 3% Na w/w. TPR profiles of crystalline compounds (C) have been included for comparison: (a) $Na_2MoO_4 \cdot 2H_2O$, (b) $Na_2Mo_2O_7$, (c) MoO_3.

Mo_2O_7, and $Na_2MoO_4 \cdot 2H_2O$), are shown in Fig. 2. For all the bulk compounds reduction starts at high temperatures (>830 K), and melting occurs in the reduction temperature range. However, there are significant changes in these reduction profiles (see Fig. 2C) that may be associated to the different environment of molybdenum atoms in the compounds. Thus, isolated $[MoO_4]$ units in $Na_2MoO_4 \cdot 2H_2O$ are less reducible than octahedral $[MoO_6]$ units in MoO_3. Only one reduction peak with a maximum temperature, T_m, ca. 1170 K is shown by the first compound, and the hydrogen uptake is lower (ca. 70%) than the value expected for the reduction of all the Mo(VI) to Mo(0), while MoO_3 has a first peak at T_m 1040 K, a complex profile after its melting at 1068 K, and Mo(VI) is reduced to Mo(0) up to 1200 K. An intermediate behavior is shown by $Na_2Mo_2O_7$ where $[MoO_6]$ and $[MoO_4]$ units built the infinite chain structure of the $Mo_2O_7^{2-}$ anion. Reduction starts near the melting temperature (885 K) of this compound with two reduction peaks at T_m ca. 950 and 1040 K, and only ca. 50% of the hydrogen uptake expected for the reduction of all the molybdenum present in this sample is measured up to 1100 K, thus indicating an incomplete reduction at this temperature limit.

In all supported samples, the onset of the reduction process occurs at lower temperatures than for the bulk compounds, thus suggesting the spreading and dispersion of molybdenum-containing compounds on the support surface. High-temperature reduction processes are more difficult to assign. Highly dispersed polymolybdate species on TiO_2 supports, detected by Raman and IR spectroscopy, have been reported to reduce at temperatures higher than 950 K (26). Alternatively, an increase in the relative intensity of these high-temperature reduction maxima could be explained by agglomeration of MoO_3 crystals, by growing of chain anions similar to those existing in $Na_2Mo_2O_7$, or by formation of isolated MoO_4^{2-} species, since all of them have reduction processes at temperatures higher than 830 K as shown for the bulk compounds.

The addition of sodium changes the TPR profile of the supported molybdenum species. Thus, for samples calcined at 773 or 1100 K, the reducibility of the supported phase decreases as the sodium content is increased as shown by the higher onset temperatures of the reduction processes for the sodium-doped samples. A decrease in the reducibility of supported molybdena when doped with alkaline metals has been previously reported (16).

TPR profiles in Fig. 2A for samples calcined at 773 K show that the addition of 1% Na w/w to MoO_3/TiO_2 does not affect in a significant way the amount of supported molybdenum reduced at temperatures lower than 830 K; therefore, we may assume that the amount of dispersed Mo-species reducing at low temperature is similar in both samples. However, different TPR line shapes again suggest changes in the nature of supported molybdenum species when going from the Na-free sample to the 1% Na-doped sample. Besides this, a higher intensity of the reduction peak at ca. 1100 K could be ascribed to the formation of isolated MoO_4^{2-} units, previously detected by FTIR data. Doping with 3% Na w/w clearly decreases the amount of dipersed molybdenum reducing at temperatures lower than 830 K. New TPR maxima appear at 900–1000 K, which could be ascribed to the formation of bulk $Na_2Mo_2O_7$, by comparison with the TPR profile of this compound and in agreement with XRD and FTIR data. The simultaneous presence of isolated MoO_4^{2-} species in this sample, enhancing the reduction peak at ca. 1100K, cannot be discarded.

Calcination at 1100 K leads to Na-doped samples with more defined reduction profiles (Fig. 2B), suggesting a lower heterogeneity of the supported species after this high-temperature calcination treatment. The amount of molybdenum reducing at temperatures lower than 830 K, although significant in both samples, decreases when compared to those found in the samples calcined at 773 K, thus suggesting a lower amount of dispersed Mo-species that reduce at low temperature after the high-temperature calcination. TPR maxima between 900 and 1100 K, ascribed to bulk $Na_2Mo_2O_7$, are now clearly resolved and more intense in the sample doped with 3% Na w/w, thus pointing to a further progress of the reactions between Mo and Na that were initiated during calcination at 773 K, probably following the segregation of Mo–Ti–Na compounds due to the strong decrease of surface area after calcination at 1100 K. However, as calcination at high temperature leads both to rutilization and sintering of the support, changes observed in the supported phases cannot

be undoubtedly related to one of these effects only. Again, in these samples isolated MoO_4^{2-} could be contributing to the high-intensity reduction maximum at 1100 K. These species were detected by FTIR in the 1% Na sample calcined at 1100 K.

EXAFS

Experimental results reported above indicate that highly dispersed molybdena species are formed on the TiO_2 support for all the samples under study. These highly dispersed species are dominant in the Na-free and the 1% w/w Na-doped samples, as shown by their XRD patterns. Doping the support with 3% Na w/w clearly leads to the formation of crystalline $Na_2Mo_2O_7$, but a fraction of molybdena still remains as well-dispersed species, as suggested by the presence of low-temperature reduction peaks in the TPR profiles. The structure of the dispersed phases is not clearly stated, although the formation of poorly crystallized $Na_2Mo_2Mo_2O_7$ chains and/or isolated MoO_4^{2-} units upon Na addition is suggested by FTIR and TPR data. In order to elucidate the structure of dispersed molybdena, EXAFS spectra for the supported samples calcined at low temperature have been measured and compared with those of bulk MoO_3 and $Na_2MoO_4 \cdot 2H_2O$, compounds where molybdenum atoms are in well-defined octahedral or tetrahedral local environments.

EXAFS data for crystalline MoO_3 and $Na_2MoO_4 \cdot 2H_2O$, and their uncorrected k^3-weighted Fourier transforms (FT) over the data range $3.6 < k < 15.0$ Å^{-1}, are shown in Fig. 3. The radial distribution function derived from the EXAFS spectrum of sodium molybdate ($Na_2MoO_4 \cdot 2H_2O$) contains only a main peak (1.25 Å, uncorrected) that has been ascribed (10, 27) to four oxygen neighbors at 1.772 Å, according to its structure determined by X-ray diffraction (28) and the existence of tetrahedral $MoO_4^=$ species in this compound. As shown in Fig. 3, EXAFS oscillations for MoO_3 are much more compli-

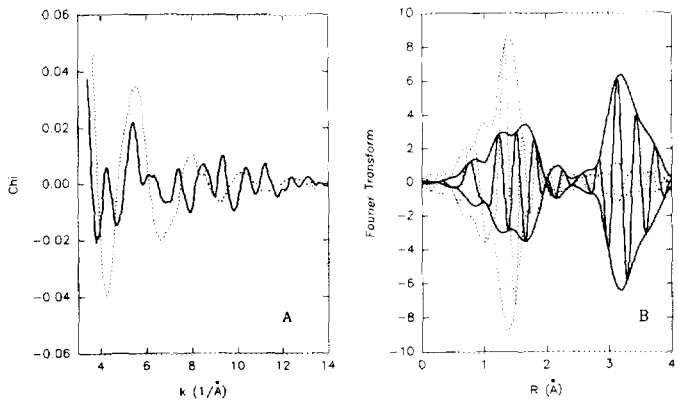

FIG. 3. Unfiltered EXAFS oscillations (A) and associated k^3-weighted Fourier transforms (B) for the crystalline compounds. Solid lines, MoO_3; dotted lines, $Na_2MoO_4 \cdot 2H_2O$.

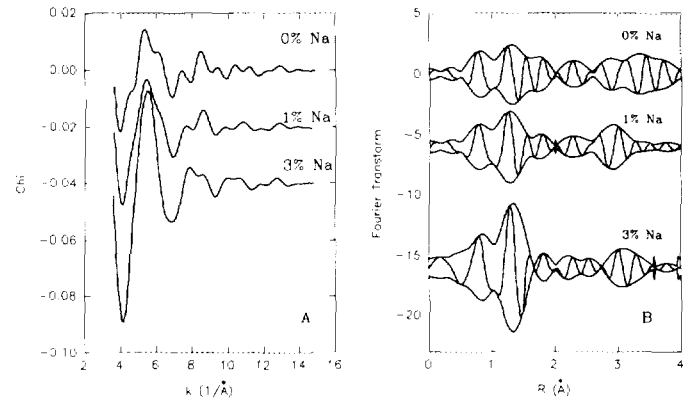

FIG. 4. Unfiltered EXAFS oscillations (A) and associated k^3-weighted Fourier transforms (B) for MoO_3/TiO_2 supported samples calcined at 773 K.

cated, giving rise to peaks centered at 1.5 and 3.1 Å in the uncorrected k^3-weighted FT. The first maximum has been ascribed to Mo–O contributions in the distorted [MoO_6] octahedra that built the MoO_3 structure, while the peak at 3.1 Å is mainly due to Mo–Mo absorber–backscattering pairs (10).

Figure 4 includes the EXAFS oscillations for MoO_3/TiO_2 supported samples calcined at 773 K and their uncorrected k^3-weighted FT ($3.6 < k < 15$ Å^{-1}). Comparison of these FT with those for the crystalline compounds (Fig. 3) shows that the regular structure at long range existing in MoO_3 (peak centered at 3 Å) has almost vanished in the supported samples. The local order of oxygen around the Mo atoms is maintained, leading to a complex maximum centered at 1.5 Å, which seems to be intermediate between those for the known structures of the crystalline compounds (distorted [MoO_6] octahedra in MoO_3, regular [MoO_4] tetrahedra in $Na_2MoO_4 \cdot 2H_2O$], suggesting that the local structure around Mo atoms in our supported samples is intermediate between the limiting situations that exist in the crystalline compounds.

EXAFS data were analyzed, as described below, by using experimental backscattering amplitude and phase functions for the Mo–Mo and Mo–O absorber–backscatterer pairs obtained from the EXAFS spectra of MoS_2 and $Na_2MoO_4 \cdot 2H_2O$, respectively. The coordination numbers and distances used for both reference compounds are given in Table 4, which also includes the data ranges employed in the analysis of experimental spectra.

Crystalline MoO_3. The radial distribution function for bulk MoO_3 (Table 5) as calculated from XRD data (30) is complex. Two well-resolved contributions in the EXAFS function are expected, one of them corresponding to six Mo–O absorber–backscatterer pairs at distances ranging from 1.671 to 2.332 Å, and the second corresponding to six Mo–Mo and six Mo–O pairs in the 3.473–3.963 Å range. Analysis of the first peak (R = 0–2 Å) in the FT,

TABLE 4

Ranges in EXAFS Data Analysis

Sample	Contribution	N	R(Å)	FT range Forward/k(Å^{-1})	FT range Inverse/R(Å)
MoS_2	Mo–Mo	6	3.16[a]	3.16–24.48	2.40–3.22
$Na_2MoO_4 \cdot 2H_2O$	Mo–O	4	1.772[b]	3.6–16.0	0.3–2.5
MoO_3				3.60–14.29	0.6–4.0
Mo/Ti/0/773				3.64–14.86	0.6–4.0
Mo/Ti/1/773				3.64–14.60	0.6–4.0
Mo/Ti/3/773				3.54–14.72	0.5–4.0

[a] Ref. (29).
[b] Ref. (28).

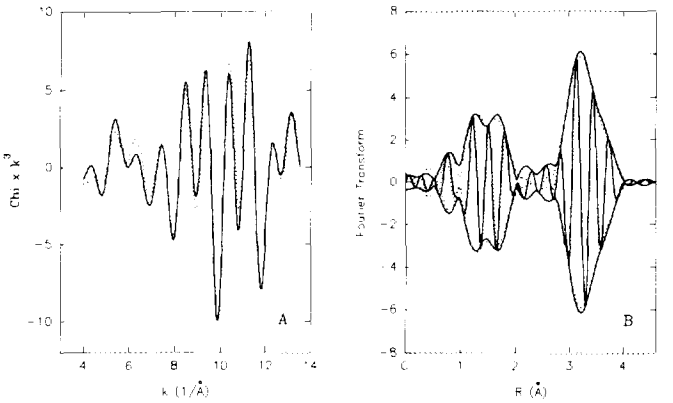

FIG. 5. Filtered EXAFS oscillations (A) and associated k^3-weighted Fourier transforms (B) for crystalline MoO_3. Solid lines, experimental data; dotted lines, best fit functions.

previously reported by Mensch *et al.* (10) and ourselves (31), simulates the [MoO_6] distorted octahedron by equal number of oxygen atoms at three different distances, yielding total coordination numbers of 5.3 O/Mo (10) and 6.0 O/Mo (31) up to 2.5 Å, in good agreement with crystallographic data. No attempt to analyze higher shell contributions has been made in these two papers. Recently, Kisfaludi *et al.* (27) modelled the EXAFS spectrum of a MoO_3/Al_2O_3 physical mixture without calcination, which they claim only contains pure MoO_3. The reported spectrum (Δk = 4.5–13.3 Å^{-1}) and its FT (ΔR = 0–4 Å) are very similar to that shown in Fig. 4, and nine shells are employed by these authors in the fit, although reported coordination numbers do not correspond with crystallographic data. Up to 2.5 Å, a total O/Mo ratio of 3.9 at five different distances is given, while an additional 9.4 O/Mo and 18.2 Mo/Mo are fitted at longer distances.

In order to check the feasibility of obtaining information about first and higher shells in MoO_3-supported systems, the EXAFS spectrum of bulk MoO_3 has been analyzed up to 4 Å by best fitting in k- and r-spaces, with a k^3-weighting scheme. The number of shells employed has been kept to the minimum possible to get a good fit of the experimental data; therefore, only three distances have been employed to model distorted [MoO_6] octahedra as was done in Refs. (10, 31). An excellent fit of the experimental data (Fig. 5) is obtained for the set of parameters included in Table 5. The radial distribution up to 2.5 Å has been previously reported by us (31), and Mo–O distances and coordination numbers are in excellent agreement with crystallographic data in this range. Higher shell contributions can be modelled by Mo–Mo pairs at three different distances (3.45, 3.71, and 4.03 Å), yielding a total coordination number of 6.8 Mo/Mo, also in agreement, within experimental error, with Mo–Mo distances and coordination numbers as determined from crystallographic data. Mo–O contributions at R values longer than 3 Å seem to be missing in the EXAFS fit done with a k^3-weighting scheme. This is not surprising, since oxygen is a light backscatterer and gives rise to low amplitude oscillations at distances of ca. 4 Å. These oscillations scarcely contribute to those much more intense due to the heavy Mo backscatterers at similar distances.

TABLE 5

Crystallographic Data (30) and EXAFS Parameters for MoO_3

XRD		EXAFS fit			
R(Å)	N	R(Å)[a]	N[a]	$\Delta\sigma^2 \times 10^3$	$\Delta E°$(eV)
1.671, 1.734	2 O	1.69	1.9	1.7	8.5
1.948	2 O	1.96	2.1	0.3	6.7
2.251, 2.332	2 O	2.26	2.0	5.9	4.2
3.437	2 Mo	3.45	1.9	1.2	1.2
3.553	4 O	—	—	—	—
3.696	2 Mo	3.71	2.4	2.6	19.6
3.764	2 O	—	—	—	—
3.963	2 Mo	4.03	2.5	3.4	9.3

[a] Estimated errors for coordination numbers (N) and shell distances (R) are ±15% and ± 0.02 Å, respectively.

Supported samples. Figure 6A shows isolated Mo–O first shell contributions for the supported samples, as compared to those obtained for the known structures of the crystalline compounds (distorted [MoO_6] octahedra in MoO_3 and regular [MoO_4] tetrahedra in $Na_2MoO_4 \cdot 2H_2O$), again suggesting that coordination by oxygen of the molybdenum atoms in the supported samples is intermediate between the limiting situations in the crystalline compounds. To assess this first guess, theoretical EXAFS spectra for different mixtures of [MoO_4] and distorted [MoO_6] units have been calculated (Fig. 6B) using the sets of parameters previously determined for MoO_3 and $Na_2MoO_4 \cdot 2H_2O$. Comparison of experimental and theo-

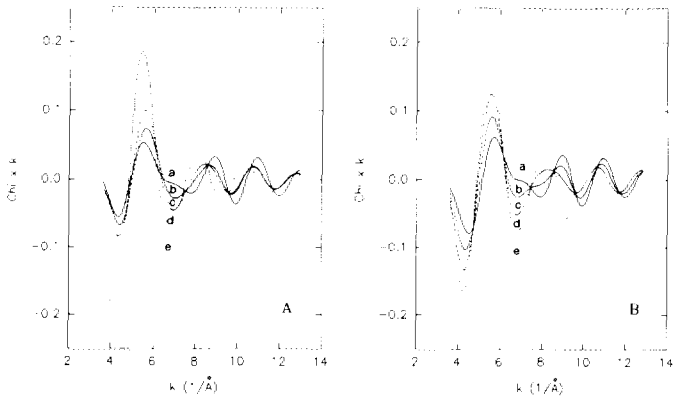

FIG. 6. (A) Isolated EXAFS oscillations for Mo–O contributions: (a) MoO_3, (b) Mo/Ti/0/773, (c) Mo/Ti/1/773, (d) Mo/Ti/3/773, (e) $Na_2MoO_4 \cdot 2H_2O$. (Fourier filtering: forward Fourier transform corrected by Mo–O phase shift and backscattering amplitude, Δk = 3.6–13.9 $Å^{-1}$; inverse Fourier transform, ΔR = 1.4–2.3 Å.) (B) Theoretical EXAFS oscillations for different fractions (x) of $[MoO_4]$ units: (a) x = 0, (b) x = 0.4, (c) x = 0.6, (d) x = 0.8, (e) x = 1. The remaining molybdenum atoms are in octahedral coordination.

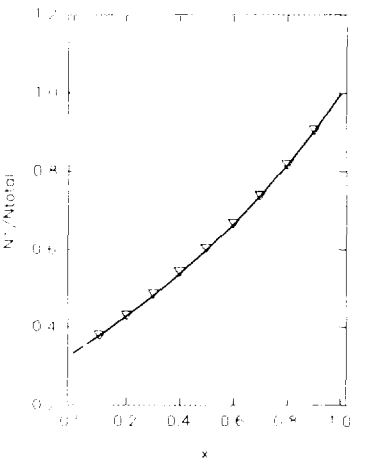

FIG. 7. Effect of increasing fractions of Molybdenum atoms in tetrahedral coordination on the ratio between the oxygen coordination number at ca. 1.7 Å and the total O/Mo coordination number.

retical spectra in Fig. 6 demonstrates that changes in the first shell spectra could be explained on the basis of an increase in the fraction of $[MoO_4]$ species in the supported samples as the Na content is increased.

The relative fractions of both coordination types for molybdenum atoms have been determined by a best-fit analysis of the experimental spectra. In crystalline $Na_2Mo_2O_7$, detected by XRD in the sample doped with 3% Na w/w, Mo–O distances in the $[MoO_6]$ units range from around 1.70 to 2.2–2.3 Å, as in other polymolybdates and also in MoO_3 (25b). Therefore Mo–O distances determined in the EXAFS analysis of bulk MoO_3 (1.69, 1.96, 2.26 Å) are adequate as a first guess to model the distorted $[MoO_6]$ units. Mo–O bond distances in the isolated $[MoO_4]$ units of $Na_2MoO_4 \cdot 2H_2O$ have a mean value of 1.77 Å, a similar value to that found in the $[MoO_4]$ tetrahedra of crystalline $Na_2Mo_2O_7$ where they range from 1.71 to 1.79 Å (25b). An analysis of the simulated EXAFS spectra in Fig. 6B shows that the 1.77-Å bond of the tetrahedral structure can be promediated with the medium bond length at 1.69 Å of the octahedral units. Increasing the relative fraction of molybdenum atoms in tetrahedral coordination (x) will lead to a slight increase of the first Mo–O bond length from 1.69 Å for x = 0 to 1.77 Å for x = 1 and simultaneously to increased values of the coordination number at ca. 1.7 Å (N_1) and to a decrease of the total Mo–O coordination number (N_t). Results for the N_1/N_t ratio obtained from the analysis of the simulated EXAFS spectra are plotted in Fig. 7, showing that this parameter could be used to determine the fraction of $[MoO_4]$ units (x) in the supported samples. In fact, it can be easily demonstrated that both values should be related through the expression $N_1/N_t = (2 + 2x)/(6 - 2x)$.

Isolated Mo–O oscillations for the supported samples in Fig. 6A have been analyzed by best-fit techniques in k- and r-spaces following k^1- and k^3-weighting schemes. Starting with the set of parameters obtained for bulk MoO_3, N and $\Delta\sigma^2$ were first allowed to vary and $\Delta E°$ and R were then taken in the refinement. Best fit parameters for Mo–O shells are collected in Table 6. The results obtained for this first shell analysis have been taken as initial parameters for a more complete analysis up to 4 Å in r-space. Mo–Mo contributions were added by starting

TABLE 6

Results of EXAFS Analysis for MoO_3/TiO_2 Samples

% Na	Shell	R(Å)[a]	N[a]	$\Delta\sigma^2 \times 10^3$	$\Delta E°$(eV)	% Td
0	O	1.72	2.0	2.1	3.4	
	O	1.96	1.6	2.6	8.1	
	O	2.26	1.3	10.7	8.6	15
	Mo	3.31	1.0	4.2	16.6	
	Mo	3.71	1.4	2.7	19.6	
	Mo	4.05	0.6	0.5	3.4	
1	O	1.72	2.7	3.1	7.1	
	O	1.95	1.7	3.7	8.8	
	O	2.21	1.2	9.1	4.4	30
	Mo	3.28	1.2	2.9	14.2	
3	O	1.76	3.8	2.1	0.6	
	O	1.96	0.7	1.3	3.5	
	O	2.21	0.6	4.9	6.4	71
	Mo	3.38	0.6	0.7	10.0	

[a] Estimated errors for coordination numbers (N) and shell distances (R) are ±15% and ±0.02 Å, respectively.

with shell parameters as obtained for MoO_3. After refining the amplitudes, the shell radii as well as the ΔE_0 shifts were taken into the refinement. The calculated parameters are included in Table 6 and best fit results for the EXAFS oscillations filtered in the 0–4 Å range are plotted in Fig. 8.

A small amount (15%) of tetrahedrally coordinated molybdenum atoms are already present in the Na-free sample, and this value increases to 71% when the amount of doping Na is increased. This increase in the fraction of molybdenum atoms in tetrahedral coordination is accompanied, as expected, by a slight lengthening of the first Mo–O bond.

Mo–Mo coordination numbers included in Table 6 for supported samples are at least 60% lower than those calculated from the EXAFS analysis of crystalline MoO_3 (Table 4), indicating that spreading of molybdena on the support has been effective. As in crystalline MoO_3, three different Mo–Mo distances are found in the Na-free supported sample, although there is a significant shortening of the first Mo–Mo distance (from 3.45 Å in MoO_3 to 3.31 Å). Mo–Mo distances shorter than those found in MoO_3 have been reported in the radial distribution of the heptamolybdate anion (27), as determined from XRD data (33). Another significant finding is that Mo neighbors at 3.71 and 4.03 Å, existing in crystalline MoO_3, are maintained in the supported sample with lower coordination numbers, although the coordination number of the longest distance seems to be preferentially decreased. When the support is doped with increasing amounts of sodium, a further decrease in the Mo–Mo coordination number is noted, and only the shortest Mo–Mo distance (ca. 3.3 Å) is kept.

It should be noted that experimental and calculated uncorrected FTs for all the supported samples show significant differences between 2 and 2.5 Å. These differences could be fitted by ca. 0.6 oxygen atoms at 2.75 Å, a value close to a long Mo–O distance previously reported by Kisfaludi *et al.* (27) in MoO_3/Al_2O_3 samples (oxygen atoms at 2.78 Å). However, the presence of differences in the 2–2.5 Å region in the fit of bulk MoO_3 (see Fig. 5), where this distance is absent in the radial distribution function calculated from crystallographic data, makes this contribution doubtful on our view. If any, the alternative ascription to Al backscatterers located on the support made by Kisfaludi *et al.* should be discarded since this Mo–O radius almost exactly coincides when MoO_3 is supported on Al_2O_3 or TiO_2.

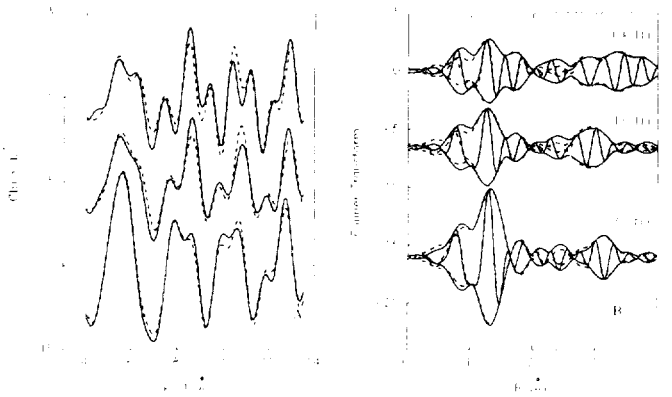

FIG. 8. Filtered EXAFS oscillations (A) and associated k^3-weighted Fourier transforms (B) for MoO_3/TiO_2 supported samples. Solid lines, experimental data; dotted lines, best fit functions.

DISCUSSION

Structure of MoO_x Moieties Supported on Undoped TiO_2

EXAFS results indicate that molybdenum atoms are mainly in octahedral coordination when supported onto the undoped TiO_2, and only a small fraction of them (ca. 15%) change their coordination to tetrahedral over this support. This result is in agreement with that reported by Shimada *et al.* (9), who found low fractions (13–28%) of molybdenum atoms in tetrahedral coordination in MoO_3/TiO_2 samples. However, these authors do not find significant contributions of Mo–Mo absorber–backscatterer pairs to the EXAFS spectra of their samples and suggest that, although the main surface species are polymolybdate as deduced by Ng and Gulari (14) from the analysis of laser raman and IR data, they should be highly disordered. The analysis of the EXAFS spectra in our MoO_3/TiO_2 sample gives a contribution of Mo–Mo absorber–backscatterer pairs ca. 60% lower than that found in bulk MoO_3. This result and those obtained by the other techniques indicate that the spreading of molybdena over the surface of the support has been effective, but information about the degree and type of condensation of $[MoO_6]$ units can be extracted from EXAFS data.

In the structure of bulk MoO_3 (Fig. 9), three different Mo–Mo distances can be identified. As shown in the figure $[MoO_6]$ units share edges to form zigzag rows along the *C*-axis of the crystal. Within these rows the two shorter Mo–Mo distances of 3.437 and 3.696 Å are found and correspond to $[MoO_6]$ units that share edges and vertex, respectively. Formation in the supported sample of these $[MoO_6]$ zigzag rows with a limited number of units between 3 and 8 will lead to Mo/Mo coordination numbers between 1.3–1.7 and 0.7–1.5 for the first and second Mo–Mo distances, respectively, thus explaining the experimental coordination numbers around one found at these two distances. Shortening of the first Mo–Mo distance when going from bulk MoO_3 to the TiO_2-supported sample is similar to that reported for ammonium heptamolybdate (27) from XRD data. In bulk MoO_3 (see Fig. 9),

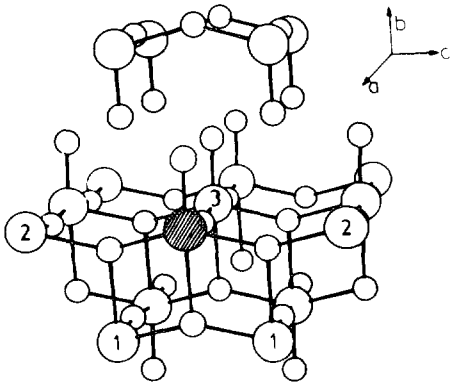

FIG. 9. Structure of bulk MoO_3 showing the different Mo–Mo distances. Large circles are molybdenum atoms and small circles are oxygen atoms. Mo neighbors around the shadowed molybdenum atom are at 3.437 Å (1), 3.696 Å (2), and 3.963 Å (3).

the zigzag rows of molybdenum atoms are joint along the *a*-axis direction by sharing vertex between the $[MoO_6]$ units, thus forming the layers in the MoO_3 structure, and the longest Mo–Mo distance (3.963 Å) is found in this direction. In the Na-free supported sample the lowest Mo/Mo coordination number is obtained at this distance from EXAFS data analysis, thus suggesting that condensation of the basic $[MoO_6]$ units along the *a*-axis direction is inhibited. Therefore, the dispersed polymolybdate species formed in this sample can be modelled as small aggregates of $[MoO_6]$ units condensed by sharing edges and vertex, similar to those found along the *c*-axis direction in bulk MoO_3, which occasionally grow by sharing vertex with similar units.

Changes in the Structure Induced by Na-Doping

Doping the support with Na leads to changes in the coordination of the molybdenum atoms from octahedral to tetrahedral, as supported by EXAFS data, which indicates that the fraction of $[MoO_4]$ units increases from 0.15 to 0.71 when going from the Na-free sample to that doped with 3% Na w/w. Simultaneously the reducibility of molybdenum is decreased, as previously observed for MoO_3/Al_2O_3 samples doped with K or Cs (16). Also, a breakdown of the surface polymolybdate identified in the Na-free sample is deduced from the decrease in Mo–Mo coordination numbers in Na-doped samples. Molybdenum atoms in tetrahedral coordination should be like $[MoO_4]$ isolated units, or forming complex chains with other molybdenum atoms in octahedral coordination, similar to those found in bulk $Na_2Mo_2O_7$.

Thus, in the 1% Na w/w sample molybdena is a well-dispersed surface species and IR data suggest the formation in this sample of noncrystalline $Mo_2O_7^{2-}$ chains and isolated MoO_4^{2-} units. This result is supported by the increase in the number of molybdenum atoms in tetrahedral coordination and the decrease of Mo–Mo coordination numbers determined from EXAFS data.

In the samples doped with 3% Na w/w the formation of crystalline $Na_2Mo_2O_7$ after calcination at 773 or 1100 K is evident from XRD, IR, and TPR data; however, TPR profiles indicate that dispersed species coexist with the crystalline dimolybdate over the surface of the sample. Analysis of the EXAFS spectrum of this sample indicates that 71% of molybdenum atoms are in tetrahedral coordination. Since there are only 50% of $[MoO_4]$ units in $Na_2Mo_2O_7$ and the remaining molybdenum atoms are in octahedral coordination in this compound, the presence of isolated $[MoO_4]$ units in this sample can be inferred, although their characteristic IR band at 900 cm^{-1} should be masked by the intense spectrum of $Na_2Mo_2O_7$. $Mo_2O_7^{2-}$ chains in noncrystalline form, like those identified in the sample doped with 1% Na w/w, should be forming the disperse phase that is still present in this sample. Therefore, the structural changes induced by Na-doping at the two Na/Mo atomic ratios studied here can be summarized by an increase in the fraction of $[MoO_4]$ units over the TiO_2 support, which may share vertex with octahedral units still remaining on the surface thus forming $Mo_2O_7^{2-}$ chains. These chains are initially well dispersed, but crystallize as $Na_2Mo_2O_7$ when their number highly increases at high Na contents. Besides this, part of the $[MoO_4]$ units are isolated species on the TiO_2 support. An increase in the calcination temperature does not affect in a significant way the structure of molybdena phases, as shown by IR spectra, its main effect being to decrease the amount of well-dispersed species that are more homogeneous after the high-temperature treatment, as suggested by TPR data.

A special level of interaction between molybdenum atoms and alkaline metals at Alk/Mo atomic ratios higher than two was previously reported (16) in the study of MoO_3/Al_2O_3 samples doped with K or Cs and was ascribed to the formation of new compounds over the surface of an alumina support. Results reported here do not indicate the formation of new surface compounds at the highest Na contents, although a Na/Mo ratio higher than two is reached in the 3% Na w/w samples.

ACKNOWLEDGMENTS

The authors thank DGICYT (Projects PB89-0642, PB91-0425) and Junta de Castilla y Leon for financial support.

REFERENCES

1. Vanhove, D., Op, S. R., and Fernandez, A., Blanchard, M., *J. Catal.* **57**, 253 (1979).
2. Ono, T., Nakagawa, Y., Miyata, H., and Kubokawa, Y., *Bull. Chem. Soc. Jpn.* **57**, 1205 (1984).

3. Okazaki, S., Kumasaka, M., Yoshida, J., Kosaka, K., and Tanabe, K., *Ind. Eng. Chem., Prod. Res. Div.* **20,** 301 (1981).
4. Tanaka, K., and Tanaka, K. I., *Chem. Soc., Chem. Commun.* 748 (1984).
5. Segawa, K., Soeya, T., and Kim, D. S., *Res. Chem. Intermed.* **15,** 129 (1991).
6. Knözinger, H., In *"Proceedings, 9th International Congress on Catalysis, Calgary, 1988"* (M. J. Phillips and M. Ternan, Eds.), Vol. 5, p. 20. Chem. Institute of Canada, Ottawa, 1988.
7. del Arco, M., Carrazan, S. R. G., Rives, V., Gil-Llambías, F. J., and Malet, P., *J. Catal.* **141,** 48 (1993).
8. Eon, J. G., Bordes, E., Vejux, A., and Courtine, P., in "Proceedings, 9th Symposium on the Reactivity of Solids" (K. Dyrek, J. Haber, and J. Nowotny, Eds.), p. 603. PWN, Warnzac, 1982.
9. Shimada, H., Matsubayashi, N., Sato, T., Yoshimura, Y., and Nishijima, A., *J. Catal.* **138,** 746 (1992).
10. Mensch, C. T. J., Van Veen, J. A. R., Van Wingerden, B., and Van Dijk, M. P., *J. Phys. Chem.* **92,** 4961 (1988).
11. Jezirowski, H., and Knözinger, H., *J. Phys. Chem.* **83,** 1166 (1979).
12. Zingg, D. S., Mokovski, L. E., Tischer, R. E., Brown, F. R., and Hercules, D. M., *J. Phys. Chem.* **84,** 2898 (1980).
13. Medema, J., van Stam, C., de Beer, V. H. J., Konings, A. J. A., and Koningsberger, D. C., *J. Catal.* **53,** 386 (1978).
14. Ng, K. Y. S., and Gulari, E. J., *J. Catal.* **92,** 340 (1985).
15. Caceres, C. V., Fierro, J. L. G., Lazaro, J., Agudo, A. L., and Soria, J., *J. Catal.* **122,** 113 (1990).
16. O'Young, C. L. *J. Phys. Chem.* **93,** 2016 (1989).
17. Kantschewa, M., Delannay, F., Jeziorowski, H., Delgado, E., Eder, S., Ertl, G., and Knözinger, H., *J. Catal.* **87,** 482 (1984).
18. Fransen, T., Van Berge, C., and Mars, P., *in* "Preparation of Catalysts" (P. Delmon, P. A. Jacobs, and G. Poncelet, Eds.), p. 405. Elsevier, Amsterdam, 1984.
19. Kust, R. N. *Inorg. Chem.* **6,** 2239 (1967).
20. Dupuis, R., and Viltange M., *C. R. Hebd. Seances Acad. Sci.* **255,** 2582 (1962).
21. Joint Committee on Powder Diffraction Standards, 22–906.
22. Malet, P., and Caballero, A., *J. Chem. Soc., Faraday Trans., 1* **84,** 2369 (1988).
23. Sayers, D. E., and Bunker, B. A. "X-Ray Absorption: Principles, Applications, Techniques of EXAFS, SEXAFS and XANES" (D. C. Koningsberger, and R. Prins, Eds.), Wiley, New York, 1988.
24. Criado, J. M., and Real, C., *J. Chem. Soc., Faraday Trans. 1* **79,** 2765 (1983).
25. (a) Wells, A. F., "Structural Inorganic Chemistry," 5th ed., p. 234. Oxford Science, Oxford, 1984; (b) Wells, A. F., "Structural Inorganic Chemistry," 5th ed., p. 516. Oxford Science, Oxford, 1984.
26. Del Arco, M., Martin, C., Rives, V., Sanchez-Escribano, V., Ramis, G., Busca, G., Lorenzelli, V., and Malet, P., *J. Chem. Soc., Faraday Trans.* **89,** 1071 (1993).
27. Kisfaludi, G., Leyrer, J., Knözinger, H., and Prins, R., *J. Catal.* **130,** 192 (1991).
28. Matsumoto, K., Kobayashi, A., and Sasaki, Y. *Bull. Chem. Soc. Jpn.* **48,** 1009 (1975).
29. Dickinson, R. G., and Pauling, L., *J. Am. Chem. Soc.* **45,** 1455 (1923).
30. Kihlborg, L., *Ark. Kemi* **21,** 357 (1963).
31. Malet, P., Muñoz-Paez, A., Martin, C., Martin, I., and Rives, V., *in* "Catalysis and Surface Characterization" (T. J. Dines, C. H. Rochester, and J. Thomson, Eds.), p. 256. The Royal Society of Chemistry, Cambridge, 1992.
32. S. Hasnair, Ed., "Report on the International Workshop on Standards and Criteria in XAFS X-ray Absorption Fine Structure," p. 755 Ellis Horwood, New York, 1991.
33. Lindquist, I., *Acta Crystallogr.* **3,** 159 (1950).